

AD-A169 122

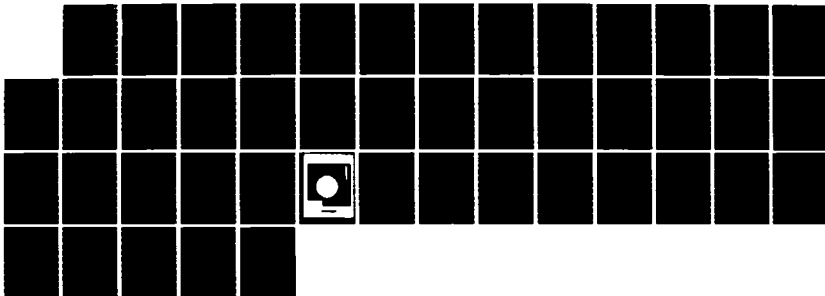
RADIOGRAPHIC DETERMINATION OF MASS AND INERTIAL TENSOR
OF ANATOMICAL SEGMENTS(U) ANCO ENGINEERS INC CULVER
CITY CA MAY 86 ANCO-1663.15 N00014-85-C-0594

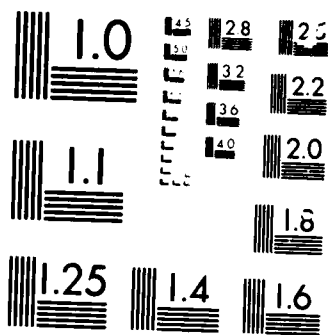
1/1

UNCLASSIFIED

F/B 6/19

NL





MICROCOPY

11701

AD-A169 122

ANCO

(Handwritten marks: a scribble, a circled 'P', and a circled '1')

REPORT

1663.15
May 1986

SBIR PHASE I FINAL REPORT

RADIOGRAPHIC DETERMINATION OF MASS AND
INERTIAL TENSOR OF ANATOMICAL SEGMENTS

Prepared for

UNITED STATES DEPARTMENT OF DEFENSE
NAVAL MEDICAL RESEARCH AND DEVELOPMENT COMMAND
Contract No.: N00014-85-C-0594

**ANCO
ENGINEERS,
INC.**

9937 Jefferson Boulevard
Culver City
California 90230-3591
(213) 204-5050
Telex: 182378
Cable: ANCOENG

(Handwritten signature)

(Faint, illegible text)

86

SBIR PHASE I FINAL REPORT
RADIOGRAPHIC DETERMINATION OF MASS AND INERTIAL
TENSOR OF ANATOMICAL SEGMENTS

Prepared for

UNITED STATES DEPARTMENT OF DEFENSE
NAVAL MEDICAL RESEARCH AND DEVELOPMENT COMMAND
TOPIC NO.: N85-57

Approval Signatures

<u>Paul Bang</u>	<u>GE Howard</u>
Project Mg./Date	Cog. Prin./Date
<u>AB Jensen</u>	<u>P. Shumick</u>
Technical QA/Date	Editorial QA/Date
<u>WD Walter</u>	
Chief Engineer/Date	

Prepared by

The Technical Staff
ANCO ENGINEERS, INC.
9937 Jefferson Boulevard
Culver City, California 90232-3591
(213) 204-5050

May 1986

Checked	Approved

ABSTRACT

The Naval Medical Research and Development Command desires to non-destructively measure the inertial properties of nonhuman primate bodies and limbs, with possible extension to humans. The results can be used in building accurate body dynamics models for crash and seat ejection studies. ANCO has investigated the use of multi-axis radiographs (X-ray photographs) of anatomical segments with high energy photons, which allows the determination of total mass, center of gravity, and the inertia tensor. This technique does not require any knowledge of the nature of the tissues studied (or their absorption coefficient) and does not require expensive CT-scan equipment. It was concluded that by using relatively inexpensive and simple equipment, the inertial properties could be determined with an accuracy of 5% to 10%, except for the off-diagonal terms of the inertia tensor where the errors could be larger. This larger error, however, is of limited concern in body dynamic studies.

Accession For	
NRIS	<input checked="" type="checkbox"/>
DDIC	<input type="checkbox"/>
USC	<input type="checkbox"/>
J	<input checked="" type="checkbox"/>
	<input type="checkbox"/>
	<input type="checkbox"/>
	<input type="checkbox"/>
	<input type="checkbox"/>
	<input type="checkbox"/>
	<input type="checkbox"/>

A-1



ACKNOWLEDGMENTS

This work was performed for the Naval Medical Research and Development Command Naval Biodynamics Laboratory under an SBIR Phase I contract. At ANCO, Dr. Paul Ibáñez was the project manager and was assisted by Dr. Karl Bernstein, Dr. Joseph Lassman, Mr. Jiri Jilek, Mr. Shankar Rao, and Mr. Kang Liu. At the Naval Biodynamics Laboratory, Mr. L. Lustik was contract monitor, who along with Dr. M. Weiss and Mr. Al Bitner provided valuable insight and direction.

TABLE OF CONTENTS

	<u>Page</u>
1.0 INTRODUCTION.....	1-1
2.0 GENERAL TECHNICAL DISCUSSION.....	2-1
2.1 Definitions.....	2-1
2.2 Derivation From Few-Scan Data.....	2-1
2.3 Measurement of Scan Data.....	2-3
2.4 Conceptual Implementation.....	2-3
3.0 X-RAY SOURCE.....	3-1
4.0 EXPOSURE TIME AND DOSE.....	4-1
5.0 EXPOSURE CONFIGURATION.....	5-1
6.0 ACCURACY.....	6-1
6.1 Discretization.....	6-1
6.2 Attenuation Sensitivity.....	6-1
6.3 Scattering.....	6-2
6.4 Calibration and Dynamic Range.....	6-5
6.5 Reading Error.....	6-5
6.6 Slicing Error.....	6-6
6.7 Photon Statistical Errors.....	6-6
6.8 Distributed Source.....	6-8
7.0 PHOTODENSITOMETER.....	7-1
8.0 SIMULATION PROGRAMS.....	8-1
9.0 EXPERIMENTS.....	9-1
9.1 Radiography.....	9-1
9.2 Test Objects.....	9-1
9.3 X-Ray Preparation.....	9-3
9.4 Gamma Radiograph Preparation.....	9-3
9.5 Preliminary Results.....	9-4
10.0 USE OF DETECTORS INSTEAD OF FILM.....	10-1
11.0 REFERENCES AND RELATED BIBLIOGRAPHY.....	11-1

1.0 INTRODUCTION

In the mechanical analysis and modeling of body response during dynamic events such as athletic activities, crashes, and military aircraft ejection, the inertial properties of various components of the body must be known. These properties are the total mass (M), the center of gravity (\bar{X} , \bar{Y} , \bar{Z}), the moments of inertia about each of three axes (I_{xx} , I_{yy} , I_{zz}) and the cross inertial terms (I_{xy} , I_{xz} , I_{yz}). Using these quantities in dynamic models allows realistic prediction of dynamic response. The Navy wishes to measure these body parameters (in humans and in experimental animals such as nonhuman primates) nondestructively and by an economical and simple procedure.

The nondestructive measurement of the mass or the inertia tensor of humans and laboratory animals has previously been carried out by others by a variety of means. These techniques include Computer Tomography (CT) [1-3], conventional radiography [4,5], ultra sound [6], and direct physical dynamic measurement [7]. Additional discussion of such techniques are found in References 8 through 21.

Huang [1] has used CT scanning to determine these inertial terms for a variety of human and nonhuman subjects to accuracies on the order of 2% to 5% (as proven by sectioning of frozen animals after the CT scans). CT scanners use X-rays with energies in the region of 65 keV; and consequently, the absorption depends somewhat ($\approx 50\%$) on the type of tissue involved (atomic composition). Thus, once the CT scans are taken, they must be reviewed and segmented (differentiate bone from muscle, for example) so that published attenuation coefficients can be applied. Once this is done, the relationship between the CT scan intensities (Hounsfield numbers) and density is established. The total mass and inertia tensor can then be easily computed from the detailed density distribution.

CT scans (and related scanning techniques) are an accurate and proven technique for inertia tensor determination. CT scans provide even more information than is desired. They can also break down the information for each component of the body (e.g., liver). Dr. Huang has informed ANCO that he can perform such analyses for about \$25,000 per specimen.

The NAVY suggested the use of higher energy X-rays (above 120 keV) since the dependence of attenuation on atomic composition is much smaller

(for example, at 120 keV Calcium attenuates about 39% more than carbon, whereas at 200 keV the difference is down to 19%, at 350 keV it is 5%, and at 600 keV there is less than 1% difference). The advantage of using higher energy X-rays (photons) is the elimination of the need to characterize the atomic composition of the tissues (this could be neglected with CT scans but could result in errors on the order of 40%). (Development of a high-energy CT system would be very costly.)

The NAVY suggested the use of a smaller number of radiograph axes than are used in CT scans (typically 100 to 300). Note that CT scans investigate "slices" by taking multiple scans through the slice for 100 to 300 different angular orientations around the normal axis of the slice and reconstructing the image by computational techniques. If the body is analyzed as a series of these slices, the full mass properties can be computed. In Section 2.0, we show that three properly conducted "conventional" radiographs in orthogonal axis provide sufficient information to compute all inertial properties (M, X, Y, Z, Ixx, Iyy, Izz, Ixy, Ixz, and Iyz). Scans in two orthogonal axes (say x,y) allow computation of M, X, Y, Z, Ixx, Iyy, Iyz, and Ixz. A scan in one axis (say x) allows computation of M, Y, Z, Ixx, and Iyz. While additional scans can provide redundancy and error reduction, ANCO does not believe many axes are required, except in the sense that as more angular axes are taken around a given axis, the information begins to approach that of a CT scan from which, as discussed above, inertial information can be extracted. The advantage of using a limited number of axes is that "conventional" radiographic methods can be used (simpler, more portable, less expensive). Note that a technique using only a few axes cannot yield separate data on internal organs except in that their contributions to the total body inertia are, of course, included. It is possible to use this method to segregate the inertial properties of large body sections (limbs, torso, head, etc.).

2.0 GENERAL TECHNICAL DISCUSSION

As mentioned in Section 1.0, the effort would involve the attempt to establish a few-axes, high-energy radiographic technique to determine inertial properties of anatomical segments.

2.1 Definitions

We assume that volume to be studied can be discretized into a fine space grid (X,Y,Z axes). At each point (Xi, Yj, Zk), we assign a uniform density ρ_i, j, k . The properties we derive are then

$$(1) \quad M = \sum_{ijk} \rho_{ijk} \Delta V \quad (\text{total mass})$$

$$(2) \quad \left. \begin{aligned} \bar{X} &= \sum_{ijk} \rho_{ijk} X_i / M \\ \bar{Y} &= \sum_{ijk} \rho_{ijk} Y_j / M \\ \bar{Z} &= \sum_{ijk} \rho_{ijk} Z_k / M \end{aligned} \right\} \quad (\text{Coordinates of the center of gravity})$$

$$I = \begin{matrix} I_{xx} & I_{xy} & I_{xz} \\ I_{yx} & I_{yy} & I_{yz} \\ I_{zx} & I_{zy} & I_{zz} \end{matrix} \quad (\text{inertia tensor})$$

$$\begin{aligned} I_{yx} &= I_{xy} \\ I_{xz} &= I_{zx} \\ I_{yz} &= I_{zy} \end{aligned}$$

$$(3) \quad I_{xx} = \sum_{ijk} \rho_{ijk} (Y_j - \bar{Y})^2 + (Z_k - \bar{Z})^2 \Delta V$$

(and similar for Iyy, Izz)

$$(4) \quad I_{xy} = -\sum_{ijk} \rho_{ijk} [(X_i - \bar{X})(Y_j - \bar{Y})] \Delta V$$

(and similar for Ixz, Izy)

2.2 Derivation From Few-Scan Data

As will be shown in Section 2.3, the X-ray scans can provide a measure of the total mass transversed by a beam through a single grid section

$$(5) \quad F_{jk} = \sum_i \rho_{ijk}$$

where F_{jk} is the total mass transversed along a grid line at location Y_j, Z_k (for all X_i). For simplicity, the ΔV has been left out. Similarly, we can

define

$$(6) \quad F_{ik} = \sum_j \rho_{ijk}$$

$$(7) \quad F_{ji} = \sum_k \rho_{ijk}$$

Assume that the F functions have been derived from three scans in orthogonal (x,y,z) directions. From Equations 1, 5, 6, and 7, we see that this information yields three independent estimates of the total mass, M

$$M = \sum_{jk} F_{jk} = \sum_{ik} F_{ik} = \sum_{ji} F_{ji}$$

From Equations 2, 5, 6, and 7, we see that this information yields two independent estimates of the center of gravity coordinates, for example

$$\begin{aligned} \bar{X} &= \sum_{ijk} \rho_{ijk} X_i / M \\ &= \sum_i X_i \sum_{j,k} (\sum \rho_{ijk}) / M \\ &= \sum_i X_i \sum_j F_{ji} / M \quad \text{or} \quad \sum_i X_i \sum_k F_{ki} / M \end{aligned}$$

(and similar for \bar{Y} , \bar{Z})

For simplicity in what follows, assume the axes have been shifted to yield $\bar{X} = \bar{Y} = \bar{Z} = 0$. From Equations 3, 5, 6, and 7, we see that this information yields two independent estimates of the moments of inertia (diagonal terms of the inertia matrix), for example

$$\begin{aligned} I_{xx} &= \sum_{ijk} \rho_{ijk} (Y_j^2 + Z_k^2) \\ &= \sum_j Y_j^2 \sum_{ik} \rho_{ijk} + \sum_k Z_k^2 \sum_{ji} \rho_{ijk} \\ &= \sum_j Y_j^2 \left(\sum_i F_{ji} \right) \quad \text{or} \quad \sum_k Z_k^2 \left(\sum_j F_{jk} \right) \\ &\quad \sum_k F_{jk} \quad \text{or} \quad \sum_i F_{ik} \end{aligned}$$

(and similar for I_{yy} and I_{zz})

Finally, from Equations 4 through 7, we see that this information yields a single estimate of the off-diagonal inertia terms, for example

$$\begin{aligned}
 I_{xy} &= -\sum_{ijk} \rho_{ijk} X_i Y_j \\
 &= \sum_{ij} X_i Y_j \left(\sum_k \rho_{ijk} \right) \\
 &= \sum_{ij} X_i Y_j F_{ji}
 \end{aligned}$$

2.3 Measurement of Scan Data

As shown in the previous section, the measurement of the various F functions (Equations 5 through 7) allows the computation of all desired properties. The F functions can indeed be measured from the attenuation of an X-ray beam through the media studied. Note if a beam of strength RI transverses a grid line (for simplicity assume a 1-cm grid), the attenuated output will be

$$\begin{aligned}
 RA &= RI e^{-\mu_1 \rho_1} e^{-\mu_2 \rho_2} \dots e^{-\mu_N \rho_N} \\
 &= RI e^{-\sum_n \mu_n \rho_n}
 \end{aligned}$$

where N is the number of cells in the grid transversed, μ_n is the attenuation coefficient for grid location n, and ρ_n is the density for grid location n.

Hence,

$$\sum_n \mu_n \rho_n = \log (RI/RA)$$

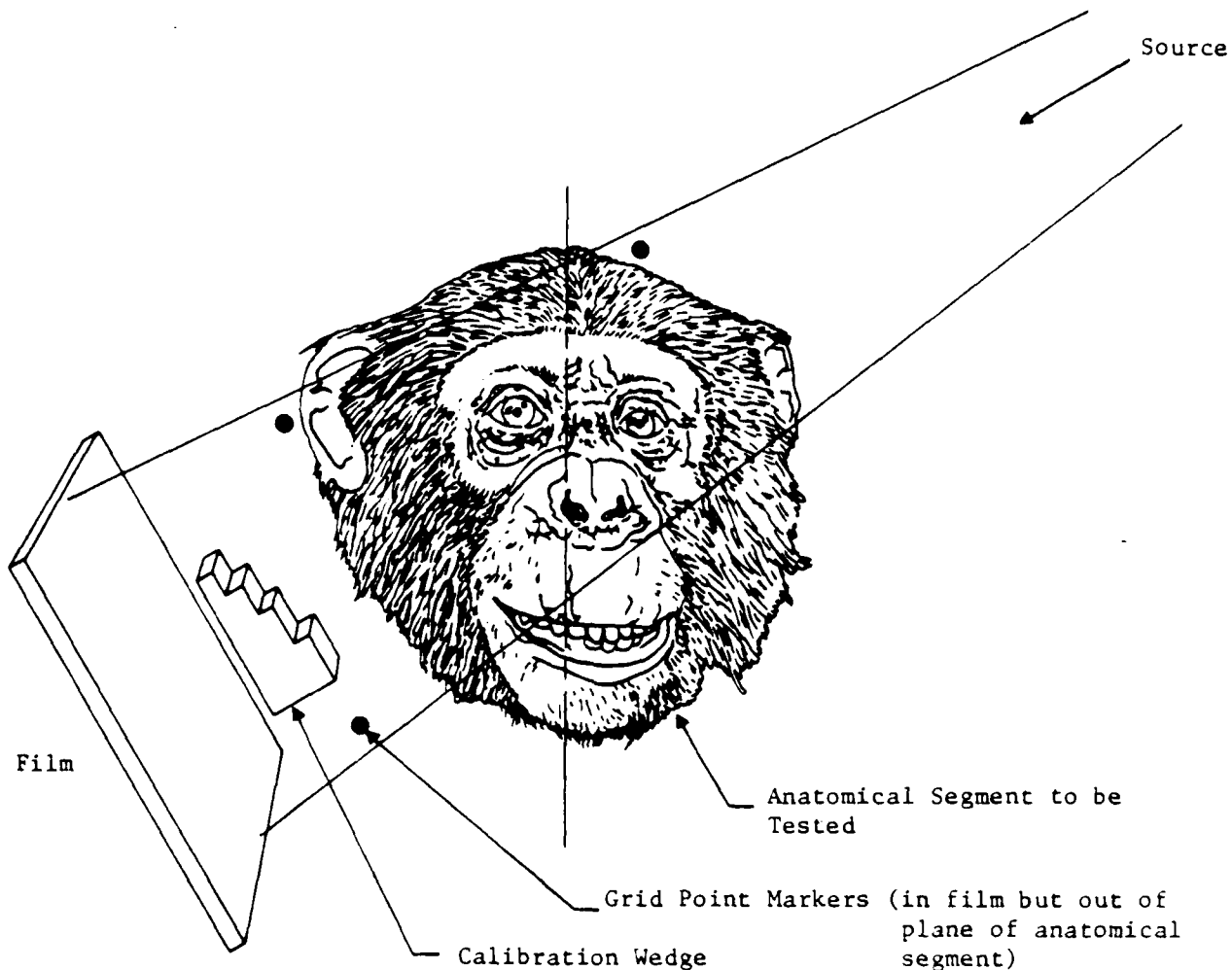
For constant μ_n , defined as μ , as is the case for higher energy photons

$$(8) F = \sum_n \rho_n = \frac{1}{\mu} \log (RI/RA)$$

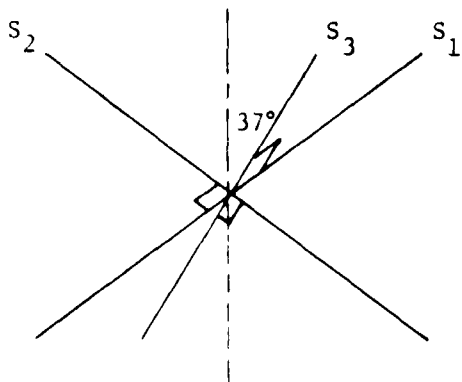
2.4 Conceptual Implementation

The production of a high-energy X-ray (photon) beam could be carried out by an X-ray tube (special units can go higher, but conventional X-ray

machines can typically reach 150 to 200 kV) or a radioactive source (e.g., Cs¹³⁷ at 662 keV energy, or Co⁶⁰ at 1.25 MeV average energy). The recording can be made by standard X-ray film or photon (X-ray, gamma ray) sensors. ANCO believes that a radioactive source and standard film is optimal, as illustrated in Figure 2.1. Note that if the inertia tensor cross-axis terms (I_{xy}, etc.) are not required, then only two scans are needed. Calibration wedges and grid point markers are present in the radiograph so as to provide for calibration and orientation. The developed radiograph films can then be scanned with a photodensitometer (over the grid, compared to the known calibration wedges) to determine the F functions.



Inertia for All Terms
 (3 scans, mutually perpendicular
 at 37° to body axis)



If Cross Terms Not Needed
 (2 scans at 90° to body axis)

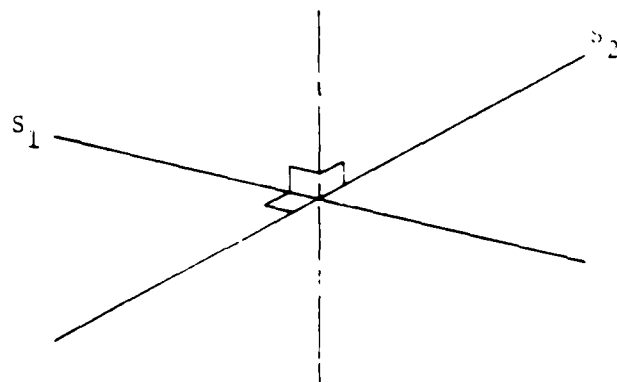


Figure 2.1: Implementation (Example)

3.0 X-RAY SOURCE

The decision must be made as to the source of the X-rays, either an X-ray tube can be used or a photon X-ray (gamma ray) source. Most commercial X-ray tubes operate below several hundred keV. Special industrial X-ray tubes can reach several MeV. All tubes provide a distributed energy source containing energies above and below their specified energy (the bulk being below).

Gamma-ray sources can provide single energy photon X-rays at high energies. Examples include Cesium 137 at .66 MeV (33 year half-life, .39 R/hr/Curie at 1-meter dosage) and Cobalt 60 (5.3 year half-life, 1.35 R/hr/Curie).

Our studies indicate that a radioactive (gamma-ray) source is preferable to an X-ray tube for the following reasons:

- The source can have a higher energy than the more commonly available tubes.
- The source energy is monochromatic (single energy), while the tube has much radiation at lower energies where absorption is atomic-number dependent. This is true even for high-energy tubes.
- The source is more easily shielded than is a machine because of the small size of the source.

4.0 EXPOSURE TIME AND DOSE

Calculations and actual testing indicate that for Agfa D-7 film (with 5-mg Pb screens and X10 intensifier) and the source placed 1 meter from the segment and screen, the following exposure time and doses are required (the sources and strengths below were those currently available to us and could, of course, be varied in future work).

<u>Source</u>	<u>Strength</u>	<u>Exposure Time (min.)</u>	<u>Dose (Roentgens)</u>
Cs137	.146 Ci	343	.32
Co60	.80 Ci	26	.47

The exposure time can be reduced by placing the source closer to the object or increasing source strength (dose will not be significantly changed). Thus, for example, use of a one-Curie source at 1/2 meter would result in an exposure time of 12.5 minutes for Cs137 and 5.2 minutes for Co60. Both this distance and source strength are practical, as several exposures (typically 3) must be made.

We are looking at total exposure times of 15 to 40 minutes; it appears feasible to hold an anesthetized animal still for this length of time. A dose of about one Roentgen should not cause the animal harm on a one- or two-time basis. It is possible that alternate films and intensifiers may further reduce these times and dosages. Larger sources could be used to reduce exposure time. Alternately, the use of more sensitive detectors, versus film, for recording measurements can reduce dosage (see Section 10.0).

5.0 EXPOSURE CONFIGURATION

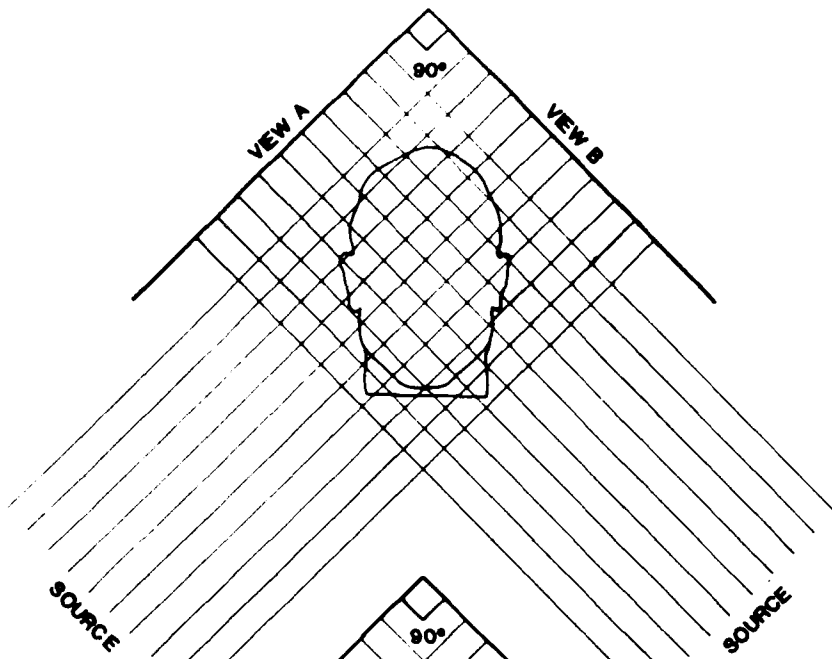
As anticipated, multiple exposures are desired. The issues to be considered are

- Can non-orthogonal views be used?
- Would more than three views be useful?
- Can exposure be made simultaneously using multiple sources?
- How can the anatomical segment be "spotted" to establish a coordinate reference?

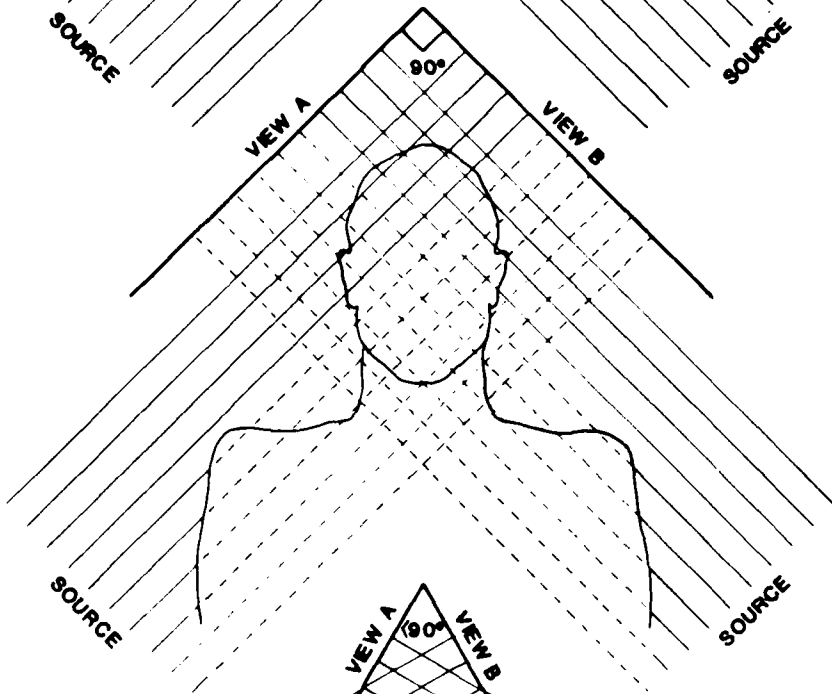
The first three points above have a common solution. Non-orthogonal views are useful so as to better isolate a given segment. For example, the head is connected to the body by the neck. If the mass properties are desired above a given reference (say a specified vertebrae) and if one could sever the head at the point and "float" it in space, one could easily take three orthogonal views, each encompassing the entire head. Since we wish to do non-destructive testing, this cannot be done. Orthogonal views of an unsevered head will result in some non-coverage and error, as illustrated in Figure 5.1.

Non-orthogonal views, also shown in Figure 5.1, reduce this error. The error could be reduced to zero by having the views in the same horizontal plane. However, they would no longer be independent, and this would lead to an inability to estimate certain mass properties. Hence, some angle, although small, must exist between all scans. Multiple scans produce redundancy and help to make up for almost dependent scans and are, consequently, potentially useful.

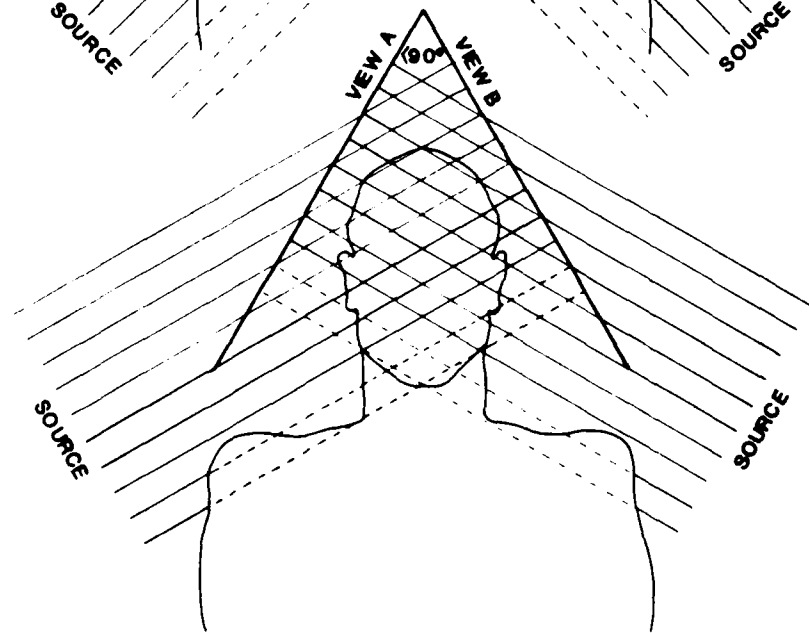
Alternately, as suggested by Mr. Lustik, if bilateral symmetry of the head (or other anatomical segment) is assumed then only two views are required for full information. Inspection of the equation for the off-diagonal inertia terms (e.g., Equation 3 in Section 2.0) shows that if, for example, the head is symmetric about the x-z plane and the center of coordinates is taken at the center of gravity then I_{xy} and I_{zy} will be zero. Thus, a view in the x direction will yield M , \bar{Y} , \bar{Z} , I_{xx} , and I_{zy} (which is zero). A view in the y direction will yield M , \bar{X} , \bar{Z} , I_{yy} , and I_{zx} (which is non-zero). We know I_{xy} is zero--from the x and y view taken together, we



Orthogonal views of a severed head have complete coverage.



Orthogonal views of an attached head can introduce errors.



Non-orthogonal views reduce this error

Figure 5.1

get I_{zz} , hence, we have the entire inertia matrix. (In fact, y and z views will also suffice.) Table 5.1 summarizes the information available from various views.

In addition to these considerations, we must concern ourselves with beam spreading. A source closer than about two meters will have a significant non-parallel beam. Non-orthogonal views, multiple views (more than three), and beam speed all introduce transformations of the data that must be accounted for. Fortunately, there is a simple technique for doing so.

Assume that any number of views are taken in any number of orientations. The views are discretely converted to give a vector, R , of measurements. For example, if five views were taken and a 20x20-cm grid used for each, then there would be 5x20x20 or 2000 measurements, and R would be a vector of length 2000. Assume also that in a convenient orthogonal coordinate system, the space containing the segment is discretely converted into cells of assumed uniform density, P . Thus, if the space is 20x20x20 cm, we can define a vector P of size 8000. Depending on the geometry of the views and the spreading ray path, each element of R is linearly dependent on some (in fact a very few) of the elements of P

$$R = TP$$

Where T is a large (2000 x 8000) matrix with most terms equal to zero. The P cannot be solved for, as there are too few equations (2000) for the unknowns (8000); and further, all the equations may not represent linearly independent data. We do not, however, wish to know P but rather certain linear combinations of P (i.e., mass, center of gravity, inertia tensor). For example, the elements of the inertia tensor can be placed in a six component vector J

$$J = UP$$

Where, for example, U is a 6 x 8000 matrix. For the moment, assume that the matrix T can be inverted and call this inversion T^{-1} .

Then

$$P = T^{-1}R$$

and

TABLE 5.1: INFORMATION AVAILABLE FROM VARIOUS VIEWS AND ASSUMPTIONS

Views	M	\bar{X}	\bar{Y}	\bar{Z}	I _{xx}	I _{yy}	I _{zz}	I _{xy}	I _{xz}	I _{yz}
X	*		*	*	*			0		0*
Y	*	*		*		*		0	*	0
Z	*	*	*				*	0*		0
X and Y	**	*	*	**	*	*	*	0	*	0*
X and Z	**	*	**	*	*	*	*	0*		0*
Y and Z	**	**	*	*	*	*	*	0*	*	0
X, Y, and Z	***	**	**	**	**	**	**	0*	*	0*

Note: Multiple asterisks indicate redundancy; 0 indicates a known zero value under assumption of bilateral symmetry about x-z plane.

$$J = UP$$

or

$$J = UTIR.$$

Where UTI is a 6 x 2000 matrix. We would, in fact, have an over-constrained system (more equations than unknowns). Note that UTI, if it existed, is only a property of the geometry of the sources and views and is independent of the properties of the segment under study.

This form of problem occurs frequently in various processing and estimation tasks [15]. In fact, a matrix, TI, can be defined that has many of the properties of the (non-existent) inverse of T. It is called the pseudo inverse (also the Penrose inverse, or singular value decomposition inverse). Without further elaboration here, note that $J = UTIR$ should provide a good estimate of the inertial properties. We know that in an orthogonal parallel scan, the answer is exact (as provided in our proposal) and feel that non-orthogonal scans with spreading beams should also yield a good estimate (as long as the angles are not too far from 90 degrees) and that multiple views (beyond three) can help. Thus, the pseudo inverse allows solution in one formalism, accounting for:

- Non-orthogonal views
- Spreading beams
- Redundant views (in the limit - a CT Scan)

The evaluation of UTI, while a lengthy computation, needs only be done once and will not change once a view geometry is chosen and maintained.

Also mentioned above are two other issues: simultaneous exposure and spotting for coordinate reference. In principle, all views could be exposed at once, thus reducing the time that an animal must be held still (anesthetized). There is no mathematical reason why the data could not be analyzed even if one view received direct exposure from more than one source. However, the effect of scattering would be greater in such a situation (because with one source, much of the scattered radiation would fall upon one of the other views, see Section 10.0). This effect will be quantified but will probably suggest against simultaneous exposure. Note that if used, simultaneous exposures reduce exposure time but not dosage.

The spotting of a coordinate reference is required. Our idea is to place a small dense object (ball bearings) at known points on the segment (e.g., vertebrae, top of head, temples, etc.), then locate these in each of the view exposures. The data-reduction computer program would then relate these to the coordinate system in which the mass properties are defined. The weight of the objects would have little effect on the calculated mass properties or, because they would be known, could be subtracted out automatically by the data-reduction computer.

6.0 ACCURACY

A primary goal is to determine the potential accuracy of this technique. Note that researchers, using a CT scanner to determine inertial properties, have, at great cost, produced results with a 5% accuracy. It is unlikely that the accuracy of our few-scan techniques would be better.

6.1 Discretization

A coarser grid will give greater error than a finer grid, but requires more computation. Discretization errors are evaluated in Section 9.5.

6.2 Attenuation Sensitivity

Even at several hundred keV and higher, there is some variation in attenuation that depends on atomic number (not just density). In Section 9.5, we present theoretical calculations of a 6.35-cm radius sphere in which the outer 1 cm is assumed to be 5% less attenuating than the inner part. This represents an upper bound on the attenuation sensitivities expected. The discretization error discussed above is present as well. In this case, mass was still predicted to within 1.3%, and the moment of inertia error is predicted to 6% (i.e., 1% different from the case in which only discretization error is present). Medical X-ray technology always has sought tissue differentiation capability, quite understandably. This has played a major role in selection of the operating voltage of the X-ray sources. In the commonly used 70 to 100 keV region, the mass absorption coefficients are quite sensitive to the atomic number of the materials in the path of the beam. One gram of calcium per square centimeter of beam cross section absorbs nearly twice the number of X-rays than are absorbed by one gram of carbon per square centimeter. As a result, bones are very prominent in medical X-rays. The contrast between bones and soft tissue also is a function of their different densities, of course, but the different chemical composition also is a significant factor.

At energies above approximately 300 keV, and up to approximately 2 MeV, the variation in these mass absorption coefficients is very much reduced. Radiographs produced in this energy range should exhibit densities quite independent of minor variations in composition. At the energies emitted by radioactive Cs¹³⁷ or Co⁶⁰, 662 keV or approximately 1.25 MeV, respectively,

the variation in mass absorption coefficient between carbon and calcium is no more than about one percent.

The only exception is hydrogen, which tends to have a coefficient about twice that of the other elements. Eight-percent hydrogen tissue has a radiographic density approximately 8% higher than it would be if the tissue had some other element substituted for the hydrogen. Fortunately, it seems unlikely that similar parts of different bodies will vary in hydrogen content by more than perhaps one percent. The same probably can be said about all but the gravest of injuries or dehydration effects in the same body. The effect of typical hydrogen content can be covered by the calibration process. Then the error associated with hydrogen content variations should not exceed about one percent.

The overall composition effect on error at Cs¹³⁷ or Co⁶⁰ energies also should be of the class of one percent, perhaps two at the very most, in concert with the numerical case mentioned above.

6.3 Scattering

X-ray or gamma ray scattering declines more rapidly with increasing energy than does absorption, but scattering remains significant throughout the practical range of energies. For cesium or cobalt sources, scattering totals approximately 1.5 times absorption. Some of the rays will be scattered in a direction that transverses the film, and statistically will contribute to the exposure. This does have the potential to limit the accuracy of the entire process, if not properly taken into account in the experiment plan or the data reduction.

The angular distribution of the scattered gamma rays is energy dependent, becoming more and more forward, relatively, at higher and higher energies. The 662-keV gammas from cesium scatter with the distribution shown below:

<u>Scattering Angle</u> <u>Range, Degrees</u>	<u>Percent of Scatters</u>	<u>Cum. Percent</u>
0 - 10	2.8	2.8
10 - 20	7.6	10.4
20 - 30	10.4	20.8
30 - 40	11.8	32.6

40 - 50	10.2	42.8
50 - 60	8.4	51.2
60 - 70	7.5	58.7
70 - 80	6.4	65.1
80 - 90	5.7	70.8
0 - 90	70.8	

Seventy percent are scattered forward, versus thirty percent backward. The energy of the scattered radiation is less than that of the original photon, declining from the undegraded value for near zero degree scatter to 288 keV at 90 degrees. Nevertheless, one must be careful to avoid massive objects immediately behind the film.

The significance of the scattering is not hard to understand. Envision an equidimensional body resting on a film cassette, and irradiated by the collimated bundle of gamma rays. Scattering events occur throughout the body. Events in the upper central region can be scattered at angles up to 30 or 40 degrees and, if they escape further scatter, arrive at a point in the film directly beneath the outer regions of the body. One third or more of this scattered radiation will fall in the image zone on the film if no action is taken to alleviate the problem. In addition, the lower energy gamma has a higher probability of interacting with the film, both because of the higher cross section at lower energy and because of the longer path through the emulsion at the slant angle.

Examination of the results of scattering in the bottom region of the film leads to the conclusion that about two-thirds of the scattered rays will fall in the image zone of the film. In this case, at least, the small angle scatters may not fall outside of the rather large resolution element that is acceptable for the current work. Overall, it appears that the scattered radiation reaching the film may be of the same order as the radiation absorbed by the body.

There are several reasons that the scattering phenomenon does not destroy medical X-rays. First and foremost, lower energy photons have a substantially lower ratio of scattering to absorption cross section. Then, when scattering does occur, the cross section is increased so sharply that absorption is virtually assured before the scattered photon can reach the film. Finally, because of the relative ease with which the low energy photons can be absorbed, filters are provided to selectively absorb those photons approaching the film at an angle indicative of scattering.

Thin absorber bars are of little value for collimating the beam from a cesium or cobalt source, and the lower absolute cross section and less favorable cross section ratio at the higher energies already has been observed. The only viable approach to high-energy absorption control is to withdraw the film from its position immediately behind the specimen. In the extreme, if the film were withdrawn a great distance, that fraction of the original collimated beam which penetrated the object would be essentially free of scattered photons by the time it reached the film. The scattering would have to be within some very small angle to remain within the image at the distant film, and very few of the scattering events involve very small angles.

Consider a 20-centimeter object withdrawn 40 centimeters (about 16 in.) away from the film. Only those photons scattered at angles less than about 14 degrees can fall in the image plane. This includes only about seven percent of those gammas scattered from the bottom of the body. The figure drops to less than three percent for scattering events in the upper part of the body. The mean is of the order of 5 percent and can be accounted for empirically in the calibration process. The residual errors probably can be held to one or two percent.

In principle, the separation could be increased to many feet, totally eliminating the scattered component of exposure, for all practical purposes. There are two potential objections. First, the density achieved on the film would decline if the level of object exposure to radiation were held constant. The "thinner" film might not be readable with the same precision; this seems resolvable. The image would be enlarged as well as less dense; the same number of unreacted gammas reach the film after penetrating the object. It should be possible to alter the instrument to read a larger section of film, corresponding to the larger size of the image. There might be some loss of exposure resolution due to the nonlinearity of the film in the low exposure region if the separation were pushed to excess.

The second concern involves growth in the defocusing of the image due to source size. The angle subtended by the source as seen from the object is projected forward to the film. The greater the objects separation from the film, the larger the image blur zone will become. However, this also must be considered relative to the enlarged image size. The blur does not

grow relative to the image, and so poses no problem in a properly redesigned experiment. The same can be said about photon statistical errors.

There seems to be little true objection to separating the film from the object, within reasonable limits. It is clear that separation of the object from the film alleviates the scattering problem. Separations of 30 to 60 centimeters may be desirable, depending on the object size. The resulting errors will be acceptable.

6.4 Calibration and Dynamic Range

All films have certain sensitivity and dynamic range. The simulations are a non-linear function of exposure and have a threshold and saturation. Thus, too small an exposure will produce a zero signal regardless of variation of the density. Too large an exposure will produce a "100%" signal regardless of the variations of density. A film and exposure time must be chosen to produce a result in the quantitative region of sensitivity, and the resulting radiograph must be capable of being quantitatively read.

Initial simulations suggest that the attenuation of the beam will vary between 9% and 90% (leaving 91% to 10% of the beam). Thus, a dynamic range of about 10 is required. The maximum attenuation is expected to equal about 1 inch of steel (the approximate equivalent path density of an X-ray through the head). To provide calibration of the film, a 1-in. steel and 1-in. aluminum step wedge have been constructed with 1/8-in. steps. As the aluminum is about 1/3 as dense as the steel, the steps provide a 24-fold dynamic range calibration in the region of interest. These wedges were used in every view of exposure. The data reduction photodensitometer reads the wedge radiographs for each view to provide a direct density calibration. It is felt that the calibration and dynamic range error can be kept below 5%. Variation of film sensitivity across a single piece of film is felt to be negligible.

6.5 Reading Error

A photodensitometer has been constructed and appears to give repeatable results to within about 3%.

6.6 Slicing Error

As discussed earlier, the radiography of any segment that is still connected to the rest of the body will cause some error due to non-overlap of the various views at the interface between the segment and the rest of the body. In Figure 6.1, a simple two-dimensional "head" with "neck" has been simulated, and the actual densities (A - including diagonal slice) are compared to ideal densities (I - perpendicular at free floating neck). As shown, the mass error is near zero. The difference in center of gravity is only 0.4% of the typical radius. The error in the diagonal inertia term is about 3%. We feel that in a three-dimensional case, the off-diagonal inertial term error would be about the same; but, as the off-diagonal term is typically much smaller, the relative error would be significant. (Remember, however, that with bilateral symmetry only two views are required, and there is no slicing error). It is concluded that, in general, the slicing error can be kept below about 3% except for the off-diagonal inertia terms.

6.7 Photon Statistical Errors

Photon statistics are satisfactory for the present purposes. The film used requires the order of 0.1 R for reasonable exposure. This indicates energy absorption of the order of 10 ergs per gram of emulsion. The emulsion thickness is of the order of 0.001 grams per square centimeter, indicating that the exposure requirement is equal to about 0.01 ergs per square centimeter. Now noting the half MeV class of the event energy, and remembering that there are approximately 600,000 MeV per erg, it is clear that the order of 10,000 events are required per square centimeter to obtain adequate exposure.

These nuclear events are random in character, and the uncertainty in number of events occurring is equal to the square root of the number, or the order of 100 events for a one square-centimeter resolution element. This indicates that the one-square-centimeter element will have a statistical error of about one percent. If the element were reduced in size, the error would increase relative to the measurement; clearly it would become significant if the resolution requirement were comparable to those of medical X-rays. However, for the present purposes, the error is quite acceptable.

Note that even if the resolution element were significantly reduced in

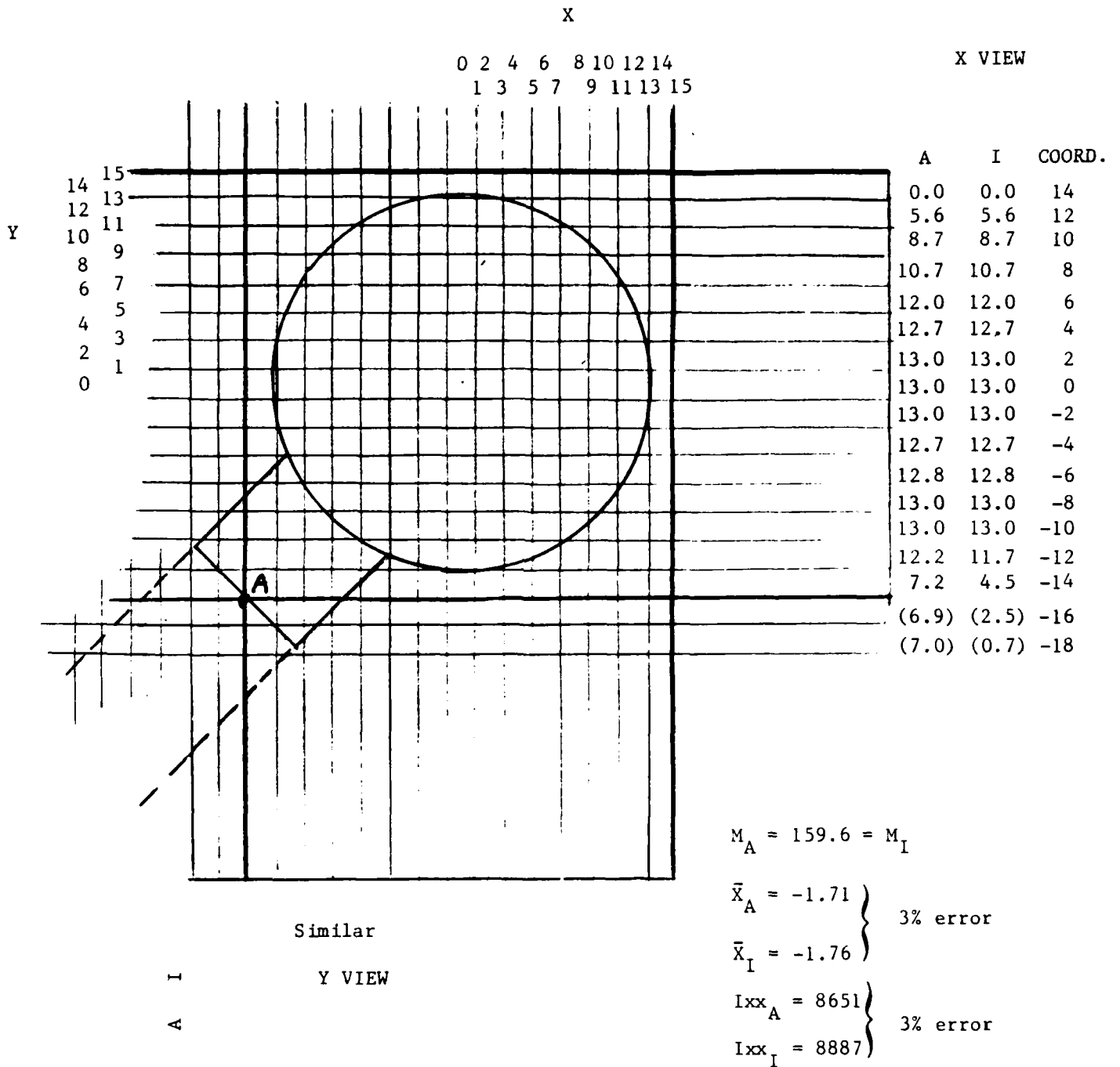


Figure 6.1

size, say to 0.1 square centimeter, the error would increase only to the order of three percent. If desired, this could be compensated by an order of magnitude increase in exposure. The film still would be readable, and the one-Roentgen exposure to the test subject probably would be acceptable. Statistical errors are not a problem.

6.8 Distributed Source

The maximum dimensions of the source, either tube target or isotopic, can be kept to less than one centimeter. The source-to-target distance is unlikely to be less than about one meter. These values imply a probable maximum angle subtended by the source at the target of 0.01 milliradians. Rays penetrating a 20-centimeter target in contact with a film will be spread over the film in proportion to this angle; and edge in the object structure will be imaged as a band 0.2 centimeters in width for the assumptions above. This is acceptable, consistent with the resolution requirements. In fact, the separation between the film and the farthest portion of the object could be increased several fold without causing unacceptable blurring for the present purposes.

7.0 PHOTODENSITOMETER

A photodensitometer has been constructed. It allows sweeping a photocell over a radiograph. The position of the photocell is measured using two orthogonal Celesco lanyard transducers (.005-in. accuracy). The transducers have + 5 volt output for + 10-in. travel. The photocell reads light intensity from a reflected light source next to the photocell. The area of illumination and sensing is approximately a 1-cm diameter circle. The photocell output is 0 to 5 volts with adjustable sensitivity.

The three signals generated (two coordinates and one intensity) are continuously read by an IBM-PC-based digital data acquisition program, ANFILM. Each 1/10 second, the data is sampled and averaged. The intensity is then assigned to the geometric grid point given by the two measured coordinates. The value is also displayed on a CRT screen grid. Thus, the photocell can be swept by hand over the film at random without regard to grid lines to "fill in" the picture. Moving slowly in significant areas results in multiple measurements and averaging of the same grid point, hence improving accuracy. Once the grid is filled in, it is written in a standard data set for future processing (called an "R" data set).

ANFILM also allows positioning of the photocell on the radiographic wedge steps for calibration. Thus, the photocell readings are directly and immediately converted to actual mass densities, cancelling out many potential errors.

ANFILM also allows positioning on the "spot" points on the segment so as to establish their exact relation to the measurement coordinate system.

8.0 SIMULATION PROGRAMS

Two other programs, ANRAY and ANSEG, have been implemented. ANRAY has the purpose of solving the equations of Section 2.2. Thus, given three "R" data sets, ANRAY calculates the corresponding mass and inertial properties. (Initially for Phase I, we are assuming three orthogonal views and parallel beams.)

The second program, ANSEG, allows the user to arbitrarily define the mass density of a segment in a three-dimensional space grid. It then calculates the mass and inertial properties and the three resulting "R" data sets. This program will be used in the simulations to evaluate grid size error, absorption variation (with atomic number) error, and dynamic range requirements. Thus, the various "R" sets from ANSEG can be analyzed by ANRAY to see how well the mass and inertial properties can be reconstructed after various error sources are introduced.

9.0 EXPERIMENTS

9.1 Radiography

Test films were prepared at typical medical X-ray energies and at 662 keV, using a Cesium 137 source. A medium-speed, high-resolution film was used in a cassette with intensifying and lead screens. Figure 9.1 is a Xerographic copy of a typical radiograph.

9.2 Test Objects

The test objects were of several classes, intended to simulate natural animal materials, to provide simple shapes, and to support density versus mass thickness calibration.

The calibration aids were manufactured from steel and aluminum. Step wedges were machined with care and were configured with eight steps, each 1/8-inch thicker than the last. The maximum thickness was one inch. The wedges are 1/2-inch wide and approximately 4-inches long. The maximum mass thicknesses of the steel and aluminum wedges are approximately 20.0 and 6.86 grams per square centimeter, respectively. The maximum steel thickness was chosen to match the mass thickness of a human head, approximately.

Spherical and cylindrical bodies were tested to allow simplified data reduction and software validity testing. Acrylic and rubber balls were used, as was a "duck-pin" bowling ball. The duck-pin ball is a 5-inch diameter sphere of an apparently uniform composition, with a density of 1.39 grams per cubic centimeter. It has a maximum mass thickness of 17.65 grams per square centimeter.

The cylindrical specimen was comprised of a lucite rod 1.75 inches in diameter by 6 inches long, with a density of 1.18 grams per cubic centimeter, inside of an aluminum tube measuring 2.125 inch o.d. by 4.125 inches long by 1.844 inches i.d.. Quarter-inch diameter holes were drilled into the ends of the lucite rod to depths of 1 and 3 inches at the two ends.

Two pseudo-natural specimens were prepared, the first comprised of gelatin with chicken bones, and some small metallic objects for composition, in a rectangular polyethylene container. The second, used later in the program, was sucrose, roughly simulating body soft tissues in atomic mass



Figure 9.1

distribution, and a simulated bone. The "bone" was a plaster of paris loaded polyethylene vial with a 2 centimeter i.d. and an inside length of 5 centimeters. The bone composition included approximately 38 percent water, resulting in a density of 1.77 grams per cubic centimeter. The mineral part of the bone is believed to have an atomic number distribution that simulates the mineral composition of true bone with adequate accuracy. The bone was placed in the center of an approximately 4-inch square by 2.5-inch high polyethylene container, which then was filled with sucrose to a density of 0.96 grams per square centimeter.

9.3 X-Ray Preparation

The initial series of radiographs were prepared with a medical X-ray unit, operating at 70 kev. The objectives of the first test series included establishment of the correct range of exposure and confirmation of the expected magnitude of the "Z" effect, the effect of atomic number on X-ray absorption at typical medical X-ray energies. About a dozen pictures were made, using the loaded gelatin and cylindrical objects described earlier. The wedges were included in all shots, and the integrated current was adjusted until qualitatively satisfactory appearing pictures were obtained for both samples. Exposures were duly noted.

9.4 Gamma Radiograph Preparation

A 143-millicurie Cesium 137 source was used in several test series. This source produces a tissue dose rate of approximately 0.5 Roentgens per hour at a distance of one foot.

As with the X-ray series, the test objects were placed directly against the cassette in the early test series. The test objects were withdrawn approximately six inches from the cassette in later experiments to confirm the validity of this technique for suppression of exposure by scattered radiation. In the final test, the wedges were left on the cassette and the sample was pulled back about six inches from the film, in an attempt to reduce confusion of the calibration densities by the radiation scattered from the sample.

9.5 Preliminary Results

Three numerical simulations and one actual radiograph were first performed. In these cases, the object of concern was the 5-inch diameter plastic sphere referred to above. The cases were

- A - Exact theoretical model
- B - Numerical evaluation of sphere using 1-cm grid size
- C - Same as A but reducing outer 1-cm shell attenuation by 5%.
- D - Reduced data from actual radiograph of plastic sphere.

The resulting mass, center of gravity (c.g.), and inertia tensor values are shown in Table 9.1. Case B (compared to Case A) shows that 1-cm grid discretization causes a 1% mass error and a 7% inertia (I_{zz}) error. The c.g. and inertia cross product (I_{xy}) error is zero. Table 9.2 shows the numerical radiographic density of this theoretical case.

Case C shows that a 5% attenuation variation in a 1-cm shell has less of an effect than the grid discretization.

Case D shows, based on the radiograph experiment, a total mass error of 13% and an inertia term (I_{zz}) error of 8%. The maximum c.g. error is about 6% of the sphere diameter. The cross product term (I_{xy}) is equal to about 2% of the diagonal (I_{zz}) term; whereas, it should be zero. In a typical human head*, the cross product terms are 3% of the diagonal terms. Hence, this cross product error (of 2%) is significant. Table 9.3 shows the measured radiographic density of this actual case (and should be compared to Table 9.2). Figure 9.1 shows a Xerographic copy of a print of this radiograph. In the original, the details of the step wedges and edges of the sphere are much clearer.

In order to further evaluate grid size and discretization effects (independent from radiographic causes of error), Case 1 through 11 of Table

* "Measurement of Mass Distribution Parameters of Anatomical Segments," by E.B. Becker, NAMRL - 1193, October 1973. I have taken his Case 3356.

TABLE 9.1: MASS AND INERTIAL PROPERTIES OF 6.35-CM RADIUS SPHERE

A - Exact Theoretical Model

$$M = \text{Total Mass} = 1.49 \text{ kg}$$

$$\text{c.g. } X = Y = 0.0 \text{ cm}$$

$$I_{zz} = 24.0 \text{ kg-cm}^2$$

$$I_{xy} = 0.0 \text{ kg-cm}^2$$

B - Numerical Evaluation with 1-cm Grid

$$M = \text{Total Mass} = 1.48 \text{ kg}$$

$$\text{c.g. } X = Y = 0.0 \text{ cm}$$

$$I_{zz} = 25.7 \text{ kg-cm}^2$$

$$I_{xy} = 0.0 \text{ kg-cm}^2$$

C - Same as B with 1-cm Shell Reduced 5%

$$M = \text{Total Mass} = 1.47 \text{ kg}$$

$$\text{c.g. } X = Y = 0.0 \text{ cm}$$

$$I_{zz} = 25.5 \text{ kg-cm}^2$$

$$I_{xy} = 0.0 \text{ kg-cm}^2$$

D - Actual Radiograph Reduction

$$M = \text{Total Mass} = 1.68 \text{ kg}$$

$$\text{c.g. } X = .37 \text{ cm, } Y = -.80 \text{ cm}$$

$$I_{zz} = 25.9 \text{ kg-cm}^2$$

$$I_{xy} = 0.6 \text{ kg-cm}^2$$

9.4 were run. In these cases, a uniform sphere of unit density and radius of 6 cm were investigated. In performing these studies, we explicitly accounted for the fact that an optical detector viewing a grid area performs an average density measurement over its field of view (spot size). Thus the only error, in principle, is that it assigns this density to the center of the grid; whereas it may not, in fact, have its center of gravity in the grid center. Because of this, the determination of mass should be exact as total mass is position independent. Review of all cases in the table shows that this is true to within 0.1%, which is probably numerical rounded-off error.

Cases 1 through 5 investigated grid size effects. The grid size was varied from 4 cm to 0.25 cm. The spot size was taken the same as the grid size. The center of the sphere was held constant at (8.8 cm). As can be seen, a 1-cm grid results in errors on the order of 1% for center of gravity position and inertia. The off-diagonal inertia, which should be zero, is, in fact, very small when compared to the diagonal terms (all inertia terms have been calculated with respect to the center of gravity). A decrease in grid size to 0.25 cm reduces errors to about 1/3% (hardly a useful improvement). An increase to 2 cm results in up to 5% error, and an increase to 4 cm yields 15% error in the inertia terms. Hence, it would appear that a 1-cm grid would suffice and keep the discretization error well below that due to other sources.

Cases 6 through 8 investigated the effect of a sphere not exactly centered on the grid. (It was initially felt that the good results and small off-diagonal inertia could be due to the symmetry of Cases 1 through 5 on the grid.) As can be seen, the nonsymmetry of the grid to sphere has little effect on the results.

Cases 9 through 11 investigated the effect of the "spot" size being different than the grid size. It would appear that a spot size about equal to the grid size gives the best result.

TABLE 9.4: DISCRETIZATION STUDY

Case	Grid Size (cm)	Sphere Radius (cm)	Spot Size (cm)	Actual				Calculated						
				M	\bar{X}	Y	Izz	Ixy	M	\bar{X}	\bar{Y}	Izz	Ixy	
1	16	1.0	6.0	1.0	905	8.0	8.0	13,030	0.0	905	7.94	7.94	13,200	-0.18
											0%	1%	1.3%	small
2	32	0.5	6.0	0.5	905	8.0	8.0	13,030	0.0	905	7.97	7.97	13,100	.012
											0%	½%	½%	small
3	64	0.25	6.0	0.25	905	8.0	8.0	13,030	0.0	905	7.98	7.98	13,000	.0035
											0%	1/3%	1/5%	small
4	8	2.0	6.0	2.0	905	8.0	8.0	13,030	0.0	904	7.87	7.87	13,600	.1500
											1/10%	2%	5%	small
5	4	4.0	6.0	4.0	905	8.0	8.0	13,030	0.0	900	7.78	7.78	14,800	-3.00
											½%	3%	15%	small
6	16	1.0	6.0	2.0	905	8.5	8.0	13,030	0.0	905	8.44	7.94	13,200	-.022
											0%	1%	1%	small
7	16	1.0	6.0	1.0	905	8.5	8.5	13,030	0.0	905	8.44	8.44	13,200	.010
											0%	1%	1%	small
8	8	2.0	6.0	2.0	905	8.5	8.5	13,030	0.0	904	8.38	8.38	13,600	-.281
											1/10%	2%	4%	small
9	16	1.0	6.0	2.0	905	8.0	8.0	13,030	0.0	904	7.88	7.88	13,600	.080
											1/10%	2%	5%	small
10	16	1.0	6.0	0.5	905	8.0	8.0	13,030	0.0	902	7.97	7.97	13,000	-1.75
											1/3%	1/3%	1/5%	small
11	16	1.0	6.0	0.1	905	8.0	8.0	13,030	0.0	899	7.99	7.99	12,800	-.125
											2/3%	1/10%	2%	small

10.0 USE OF DETECTORS INSTEAD OF FILM

While film can be used as the detection media, it has some disadvantages. These include relatively low sensitivity and the need for post-processing to digitize the data. If solid-state detectors were used, the sensitivity could be greater, and the data could be directly placed in the computer. To avoid the need for a large grid of detectors, the source could be collimated into a fan or beam and scanned, thus requiring only a line of detectors, or even a single detector. In the latter case, the data analysis would be greatly simplified, as true perpendicular parallel data could be obtained without the need of the pseudo inverse manipulation to account for beam spreading.

The data-taking computer could control the scan and pause long enough at each grid point to obtain a reliable reading, thus speeding up the data taking in areas of low attenuation. The use of a collimated beam, the same size as the grid spacing, reduces the total dose to the patient. If a scan system were used, the orientation of the patient (anatomical section) would have to be indexed by a system tied to the scanning frame. This could be accomplished, for example, by four stereotaxic indicators fixing and measuring the location of Reade's plane (defined by the auditory meatuses and the orbital notches).

The resolution requirements for the proposed density instrument are relatively low; many millimeters are acceptable, compared to the fractions of a millimeter desired for diagnostic X-rays. This suggests consideration of scintillation detectors for the current application. Because they have a mass thickness of the order of a thousand times that of an X-ray film, and absorption coefficients that are equal to that of a film emulsion of equivalent thickness, scintillation detectors will reduce the patient dose dramatically.

The output of the scintillation detector is amplified and then can be handled in several ways. The most logical approach for this program is to capture the data directly in the computer. It must be input to a computer for further processing anyway, but now one has the advantage of real-time input, without waiting for film processing and densitometer. An additional advantage of the use of this type of detection is the ability to discriminate on energy, eliminating scattered photons from the data.

The primary requirements for the detection system now are seen to be a scintillation detector, preferably with an integral photomultiplier tube, a power supply, a preamplifier and amplifier, and an interface to the computer. The electronic components are available from several suppliers, of which the best known probably is EG&G ORTEC. The detector also is available from several sources, including Harshaw and Bicron Corporation.

The detection system easily can handle data at 10,000 counts per second. A large enough fraction of these counts will be in the photopeak energy band to assure two-percent counting accuracy in one second, if the source activity is high enough. For less powerful sources, the counting period will be longer, but 10,000 scintillator events still will be sufficient. Assuming a 20-cm-square image and a 2-cm-square resolution element, the total measurement time will be 100 times the exposure time for a single element.

Two-dimensional scanning is required; the alternative of either a linear or square array of detectors is more costly and not justified for this application. The scanning can be provided in several ways, because the source, subject, and detector all are movable to some degree. The simplest approach is to provide two orthogonal linear motions, presumably a horizontal motion of the subject and a vertical motion of the detector, and equip the source with a collimator providing a vertically-oriented fan-shaped output beam. The scan then is accomplished by counting with patient and detector fixed for the required incremental time, advancing the detector and counting again, and repeating the process until the vertical array is complete. Then the subject is advanced horizontally until the next vertical zone is in position for counting, and so on until completion of the data acquisition.

The patient doses are not high, even though the beam is fan shaped instead of being confined to the size and shape of the detector. The dose can be estimated directly from the required number of counts per resolution element. At 662 KeV, approximately 730 photons per square centimeter per second gives an exposure rate of 1 milliRoentgen per hour; 2.6 million photons per square centimeter yields an integrated exposure of 1 millirem. Only 10,000 events per element or about 2,500 per square centimeter, are required. Further noting that the detector will provide photopeak counts

responding about 10 percent of the impinging photons, no more than approximately 20,000 photons per square centimeter are required to expose an element. This indicates a dose on the order of 0.01 millirem during the time of counting each element in the fan. Because the entire fan region is being exposed while each element is being counted, each element of the exposed region ultimately receives 10 times this dose, or approximately 0.1 milliroentgens. This is several orders of magnitude less than the doses experienced with typical high-resolution medical X-rays. If dose suppression were of great importance, 10-fold additional suppression could be achieved by collimating to a square beam and providing two-dimensional scanning. Assuming that fan collimation is acceptable, a Cs 137 source of 60 millicuries strength will be required to complete two views in a 20-minute period.

11.0 REFERENCES AND RELATED BIBLIOGRAPHY

1. Huang, H.K., and Suarez, F.R., "Evaluation of Cross-sectional Geometry and Mass Density Distributions of Humans and Laboratory Animals Using Computerized Tomography," Journal of Biomech., 1983, Vol. 16, No. 10, pp. 821-832.
2. Huang, H.K., and Wu, S.C., "The Evaluation of Mass Densities of Human Body In Vivo from CT Scans," Comput. Biol. Med., October 1976, Vol. 6, No. 4, pp. 337-343.
3. Reid, J.G., "Physical Properties of the Human Trunk as Determined by Computed Tomography," Arch. Phys. Med. Rehabil., May 1984, Vol. 65, No. 5, pp. 246-250.
4. West, R.R., "The Estimation of Total Skeletal Mass from Bone Densitometry Measurements Using 60 keV Photons," British Journal of Radiol., August 1973, Vol. 46, No. 548, pp. 599-603.
5. Colbert, C., Spruit, J.J., and Trotter, M., "Estimation of Gravimetric Density of Fetal Bones from Radiologic Density," Invest. Radiol., March-April 1972, Vol. 7, No. 2, pp. 102-106.
6. Thompson, T.R., and Manning, F.A., "Estimation of Volume and Weight of the Perinate: Relationship to Morphometric Measurement by Ultrasonography," Journal of Ultrasound Med., March 1983, Vol. 2, No. 3, pp. 113-116.
7. Halze, A., "A New Method for the Simultaneous Measurement of the Moment of Inertia, the Damping Coefficient, and the Location of the Center of Mass of a Body Segment In Situ," European Journal of Appl. Physiology, Vol. 34, No. 4, 1975, pp. 217-226.
8. Borkan, G.A., Hults, D.E., and Gerzof, S.G., et al, "Relationships Between Computed Tomography Tissue Areas, Thicknesses, and Total Body Composition," Normative Aging Study, Ann. Hum. Biol. (England), 1983, Vol. 10, No. 6, pp. 537-545.
9. Elsasser, U., and Ruegsegger, P., "Bone Densitometry with the Aid of Computerized Transaxial Tomography," American Journal of Roentgenol., June 1976, Vol. 126, No. 6, pp. 1275-1277.
10. Tokunaga, K., Matsuzawa, Y., Ishikawa, K., and Tarui, S., "A Novel Technique for the Determination of Body Fat by Computed Tomography," Int. Journal of Obes. (England), 1983, Vol. 7, No. 5, pp. 437-445.
11. Waibel, E., "Densitometrierung Medizinischer Rontgenaufnahmen mit Linearer Schichtdickenzuordnung," Fortschr. Geb. Roentgenstr. Nuklearmed. (Federal Republic of Germany), August 1972, Vol. 117, No. 2, pp. 207-216.
12. Elk-Nes, S.H., and Grottum, P., "Estimation of Fetal Weight by Ultrasound Measurement. I. Development of a New Formula," Acta Obstet. Gynecol. Scand. (Sweden), 1982, Vol. 61, No. 4, pp. 299-305.

13. Garrow, J.S., "Techniques for the Measurement of Human Body Composition," West Indian Medical Journal, September 1974, Vol. 23, No. 3, pp. 165-173.
14. Heymsfield, S.B., McManus, C., Smith, J., Stevens, V., and Nixon, D.W., "Anthropometric Measurement of Muscle Mass: Revised Equations for Calculating Bone-free Arm Muscle Area," American Journal of Clin. Nutr., October 1982, Vol. 36, No. 4, pp. 680-690.
15. Lawson, C.L., Hewson, R.J., "Solving Least Squares Problems," Englewood, Prentice Hall, 1974.

Reports

16. Becker, E.B., "Measurement of Mass Distribution Parameters of Anatomical Segments," Naval Aerospace Medical Research Lab, Pensacola, FL, available from National Technical Information Service (NTIS), Report #AD-A016980 NAMRL-1193.
17. Chandler, R.F., and Young, J., "Uniform Mass Distribution Properties and Body Size Appropriate for the 50 Percentile Male Aircrewmember, 1980-1990," Monroney Aeronautical Center, Oklahoma City, OK, available from NTIS, Report #AD-A142946 AAC-119-81-4.
18. Drillis, R., and Contini, R., "Body Segment Parameters, TLSP: Final Report," New York University, School of Engineering and Science, NY, available from NTIS, Report #TR-1166-03 HEW-R886.
19. Laubach, L.L., "Range of Joint Motion," Webb Associates, Yellow Springs, OH, in its Anthropometric Source Book, Vol. I, available from NTIS, Report #N79-11734 02-54.
20. Maughan, R.J., Watson, J.S., and Weir, J., "The Relative Proportions of Fat, Muscle, and Bone in the Normal Human Forearm as Determined by Computed Tomography," Institute of Environmental and Offshore Medicine, University Medical School, Aberdeen, United Kingdom.
21. Selke, D.J., Little, R.W., Hubbard, R.P., and Slonim, A.R., "Mechanical Properties of Lower Limb Tendons and Ligaments in Primates," Michigan State University, East Lansing, Department of Biomechanics, MI, available from NTIS, Report #HC A03/MF A01.
22. Young, J.W., Chandler, R.F., Snow, C.C., Robinette, K.M., Zehner, G.F., and Lofberg, M.S., "Anthropometric and Mass Distribution Characteristics of the Adult Female" (revised), Air Force Aerospace Medical Research Lab, Wright-Patterson Air Force Base, OH, available from NTIS, Report #AD-A143096 FAA-AM-83-16-REV.

END

DTIC

7-86